

Comparison of image quality of head and neck lesions between 3D gradient echo sequences with compressed sensing and the multi-slice spin echo sequence

Acta Radiologica Open
Volume 9: 1–8
© The Foundation Acta
Radiologica 2020
Article reuse guidelines:
sagepub.com/journals-permissions
DOI: 10.1177/2058460120956644
journals.sagepub.com/home/arr


Yukiko Kami¹ , Toru Chikui¹, Osamu Togao², Masahiro Ooga³
and Kazunori Yoshiura¹

Abstract

Background: Although magnetic resonance imaging (MRI) provides excellent soft-tissue contrast, long acquisition times are major disadvantages.

Purpose: To evaluate the usefulness of compressed sensing (CS) for contrast-enhanced oral and maxillofacial MRI by comparing the 3D T1 turbo field echo with compressed SENSE (CS-3D-T1 TFE) sequence with the multi-slice spin echo (MS-SE) sequence as the reference standard.

Material and Methods: Thirty patients with orofacial lesions participated in this study. The scan times for MS-SE and CS-3D-T1 TFE were 5 min 56 s and 1 min 43 s, respectively. The signal-to-noise ratio (SNR) was calculated for quantitative analysis and seven parameters (degree of lesion conspicuity, motion artifacts, metal artifacts, pulsation artifacts, quality of fat suppression, homogeneity of blood vessel signal intensity, and overall image quality) were evaluated using a 5-point scale (5 = excellent, 1 = unacceptable) by two observers for qualitative analysis. For comparisons between MS-SE and CS-3D-T1 TFE, the paired t-test was used.

Results: The SNR of CS-3D-T1 TFE was higher than or equal to that of MS-SE. The CS-3D-T1 TFE scores for motion artifacts, pulsation artifacts, and homogeneity of blood vessel signal intensity were higher than the corresponding MS-SE scores in assessments by both observers. The MS-SE scores for fat suppression were higher than or equal to the CS-3D-T1 TFE scores. There were no significant differences in lesion conspicuity, metal artifacts, and overall image quality between the two sequences.

Conclusion: CS-3D-T1 TFE imaging, less than 30% of the scan time for MS-SE, showed no image degradation while retaining equal or higher SNR and image quality.

Keywords

Magnetic resonance imaging, compressed sensing, head and neck

Received 31 March 2020; accepted 17 August 2020

Introduction

Magnetic resonance imaging (MRI) provides better soft-tissue contrast than computed tomography (CT), which plays an important role in the evaluation of the location of the lesion and its relationships with adjacent anatomical structures and also provides information about the metabolic and physiological features of tissue, thereby indicating its pathological processes (1–4).

A major drawback of MRI is the slow imaging speed. Long acquisition times introduce motion

¹Department of Oral and Maxillofacial Radiology, Faculty of Dental Science, Kyushu University, Fukuoka, Japan

²Department of Clinical Radiology, Graduate School of Medical Sciences, Kyushu University, Fukuoka, Japan

³Department of Medical Technology, Kyushu University Hospital, Fukuoka, Japan

Corresponding author:

Yukiko Kami, Department of Oral and Maxillofacial Radiology, Faculty of Dental Science, Kyushu University, 3-1-1, Maidashi, Higashi-ku, Fukuoka, 812-8582, Japan.

Email: kami@rad.dent.kyushu-u.ac.jp



artifacts, increase costs, and limit the number of patients for whom MRI is available (5). Although three-dimensional (3D) scans are preferred for MRI, two-dimensional (2D) scans are common in clinical practice because 3D scans require much longer scan times and the gradient (GRE) sequence commonly used for 3D scans is susceptible to inhomogeneity of magnetic fields. Therefore, achieving a reduction in MRI acquisition time without causing image degradation has remained a challenge.

Parallel imaging (PI) uses an array of receiver coil to collect undersampled k-space data and reconstructs full field of view (FOV) images by specialized algorithms (6). The limitation is that the acceleration factor cannot be higher than the number of coils in the array (7).

Compressed sensing (CS), a mathematical framework, provides for reconstruction of data from highly undersampled measurements, which is exploited effectively under conditions of sparsity, pseudo-random undersampling, and non-linear reconstruction (8). CS takes advantage of the fact that MR images are usually sparse in some transform domains, such as the wavelet domain, and recovers this sparse representation from undersampled data (9). Like PI, CS enables accelerated MRI acquisitions although the two approaches rely on different ancillary information.

CS and PI techniques such as sensitivity encoding (SENSE) can be combined to further reduce scan time (10). For example, the compressed SENSE is available on the Philips scanner (11). According to the report by Sartoretto et al. (12), in individual scans of six different body regions (brain, knee, lumbar spine, wrist, breast, shoulder) with compressed SENSE, a reduction in acquisition time of 23%–43% in individual sequences across 2D and 3D scans was achieved with no image degradation.

To our knowledge, there have been no previous studies in which CS has been applied to head and neck lesions. The aim of the present study was to evaluate the usefulness of CS for contrast-enhanced oral and maxillofacial MRI by comparing the 3D T1 turbo field echo with compressed SENSE (CS-3D-T1TFE) sequence with the multi-slice spin echo (MS-SE) sequence as the reference standard.

Material and Methods

Patients

This retrospective study was approved by the Institutional Review Board of Kyushu University Hospital (2019-111) and the requirement for informed consent was waived. The study plan was published on a website and the patients had the right of refusal to inclusion in this study. For the present study, we

included patients with orofacial lesions who underwent contrast-enhanced MRI including MS-SE and CS-3D-T1TFE sequences at our hospital between August 2018 and April 2019. We excluded patients with lesions that could not be defined because they were too small or showed severe metal artifacts.

A total of 30/40 patients (18 men, 12 women; mean age = 63.7 ± 17.3 years; age range = 21–84 years) were identified on the basis of the above criteria. The lesions were as follows: malignant tumors (squamous cell carcinoma [SCC], $n = 17$; malignant lymphoma [ML], $n = 2$; and osteosarcoma, $n = 1$); benign tumors (pleomorphic adenomas, $n = 2$; lymphangiomas, $n = 2$; reactive myofibroblastic lesion, $n = 1$; and desmoplastic ameloblastoma, $n = 1$); cysts (ranula, $n = 1$; epidermoid cyst, $n = 1$); and inflammations, $n = 2$.

MRI acquisition

MRI was performed using a 3.0-T scanner (Ingenia 3.0CX, Philips Healthcare, Best, The Netherlands) with a 20-channel head-and-neck coil. MS-SE was performed with the following parameters: repetition time (TR)/echo time (TE) = 431/13 ms; flip angle = 90° ; water fat shift = 1.423 pixels; bandwidth = 305.2 Hz; number of signal averaged (NSA) = 1; slice thickness = 3 mm; field of view (FOV) = 230 mm; acquisition voxel = $0.72 \times 0.89 \times 3.00$ mm; reconstruction voxel = $0.45 \times 0.45 \times 3.00$ mm; and acquisition time = 5 min 56 s. The Dixon method was used for fat suppression.

CS-3D-T1TFE was performed with the following parameters: TR = 5.6 ms; TE1/TE2 = 1.94/3.4 ms; flip angle = 14° ; water fat shift = 0.500 pixels; bandwidth = 868.1 Hz; NSA = 2; CS-Sense reduction factor = 3.05; FOV = 240 mm; acquisition voxel = $1.00/1.00/1.00$ mm; reconstruction voxel = $0.47/0.47/1.00$ mm; and acquisition time = 1 min 43 s. The Dixon method was used for fat suppression.

Both sequences were performed after administration of 0.1 mmol/kg of gadolinium-based contrast material. The order of the sequences was randomized.

Image evaluation

All data were transferred from the hospital's picture archiving and communication system (PACS, Fujifilm Medical, Tokyo, Japan) to a personal computer in the digital imaging and communications in medicine (DICOM) format for further image analysis. Each patient's CS-3D-T1TFE imaging dataset (slice thickness = 1 mm) was resampled to the MS-SE imaging dataset (slice thickness = 3 mm) using the OsiriX software (Pixmeo SARL, Bernex, Switzerland, version 10.0.3) for both datasets to be evaluated under the

same conditions: the same slice thickness; the same slice numbers; the same FOV; and the same matrix size.

Quantitative analysis

One radiologist with 10 years of experience in oral and maxillofacial radiology performed the quantitative analysis. From each dataset of 60 images (30 MS-SE and CS-3D-T1TfE images each), an axial image that clearly delineated almost maximum sections of the tongue, masseter muscles, and medial pterygoid muscles was selected, and 25-pixel circular regions of interest (ROIs) were placed on the bilateral posterior part of tongue, masseter muscles, and medial pterygoid muscles using ImageJ software (National Institutes of Health, MD, USA, version 1.51s) (Fig. 1). Particular attention was paid not to include artifacts, blood vessels, and muscular fasciae in the ROIs. The signal-to-noise ratio (SNR) was calculated from each ROI using the following equation:

$$\text{SNR} = \text{SI}/\text{SD}$$

where SI and SD are the average and SD of the signal intensity, respectively.

Qualitative analysis

Two oral and maxillofacial radiologists with 10 and 23 years of experience (Observer 1 and Observer 2, respectively) independently participated in the observer test. Both observers were blinded to the sequences analyzed. Image quality was assessed using seven parameters: degree of lesion conspicuity; motion artifacts; metal

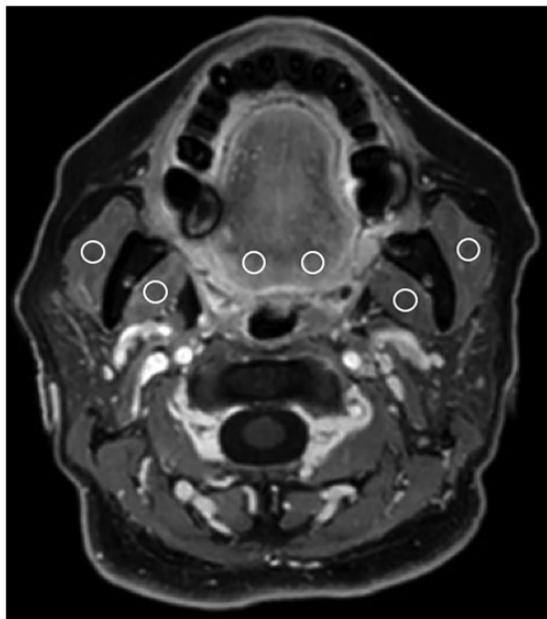


Fig. 1. 25-pixel circular regions of interest were placed on both sides of the posterior part of tongue, masseter muscles, and medial pterygoid muscles to calculate the signal-to-noise ratio.

artifacts; pulsation artifacts; quality of fat suppression; homogeneity of blood vessel signal intensity; and overall image quality. Each parameter was graded on the following 5-point scale: 5 = excellent; 4 = good; 3 = acceptable; 2 = poor; and 1 = unacceptable.

Statistical analysis

Comparisons of SNR between MS-SE and CS-3D-T1TfE and qualitative scores between the two sequences were performed using the paired *t*-test with Kaleida Graph software (Synergy Software, version 4.1.3). *P* values < 0.05 were considered significant. Inter-observer agreement in the qualitative scoring was assessed by the kappa statistic using SPSS version 21.0 (IBM Corp., Armonk, NY, USA). Agreement was interpreted based on kappa as follows: ≤ 0.20 = slight; 0.21–0.40 = fair; 0.41–0.60 = moderate; 0.61–0.80 = substantial; and 0.81–1.00 = almost perfect.

Results

MRI

The examples of MS-SE and CS-3D-T1TfE images are shown in Fig. 2.

Quantitative analysis

The mean and SD of the SNR and *P* values for MS-SE and CS-3D-T1TfE sequences are shown in Table 1. SNR of CS-3D-T1TfE was significantly higher than that of MS-SE in the right masseter muscle ($P = 0.0003$), the left masseter muscle ($P < 0.0001$), the right medial pterygoid muscle ($P = 0.0002$), and the left medial pterygoid muscle ($P < 0.0001$). There were no significant differences between the two sequences in the right posterior part of tongue ($P = 0.8945$) and the left posterior part of tongue ($P = 0.2734$).

Qualitative analysis

The individual observer grades for each parameter are listed in Table 2. For Observers 1 and 2, the scores recorded with CS-3D-T1TfE were higher than those with MS-SE for motion artifacts ($P = 0.0009613$ and $P < 0.0001$, respectively) (Fig. 3), pulsation artifacts ($P < 0.0001$ and $P < 0.0001$, respectively) (Fig. 4), and homogeneity of blood vessel signal intensity ($P < 0.0001$ and $P < 0.0001$, respectively) (Fig. 5). The scores for quality of fat suppression were significantly higher with MS-SE than with CS-3D-T1TfE for Observer 2 ($P = 0.001426$), whereas they did not significantly differ between the methods for Observer 1 ($P = 0.08307$). No significant differences were observed in the scores for lesion conspicuity ($P = 0.4888$ and

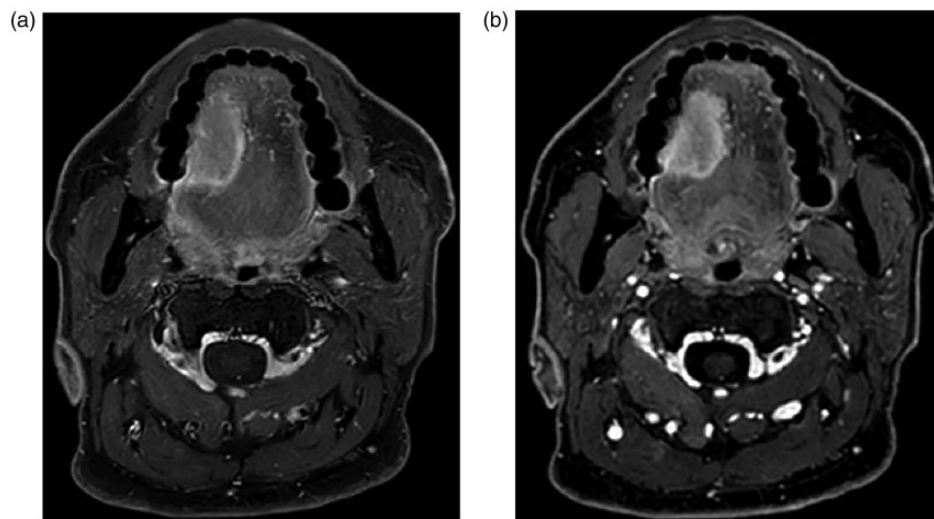


Fig. 2. A 60-year-old man with right tongue squamous cell carcinoma. Imaging was performed with the MS-SE sequence (a) and the CS-3D-T1TFFE sequence (b). Both images delineate the tongue lesions clearly. Blood vessels are more clearly on the CS-3D-T1TFFE image than the MS-SE. CS-3D-T1TFFE, three-dimensional T1 turbo field echo with compressed SENSE; MS-SE, multi-slice spin echo.

Table 1. SNR of MS-SE and CS-3D T1TFFE.

	SNR		P*
	MS-SE	CS-3D-T1TFFE	
Right tongue root	20.92 ± 7.14	20.67 ± 8.11	0.8945
Left tongue root	20.26 ± 5.69	18.75 ± 7.00	0.2734
Right masseter muscle	15.36 ± 5.99	21.99 ± 9.10	0.0003
Left masseter muscle	15.67 ± 5.37	20.85 ± 6.79	<0.0001
Right medial pterygoid muscle	13.32 ± 4.76	18.46 ± 6.39	0.0002
Left medial pterygoid muscle	12.15 ± 5.32	19.23 ± 6.81	<0.0001

Values are given as mean ± SD.

*Paired *t*-test.

CS-3D T1TFFE, three-dimensional T1 turbo field echo with Compressed SENSE; MS-SE, multi slice spin echo; SD, standard deviation; SNR, signal-to-noise ratio.

$P = 0.5725$), metal artifacts ($P = 0.1683$ and $P = 1$), and overall image quality ($P = 0.3256$ and $P = 0.6015$) for both observers. Table 3 summarizes the kappa statistics for the inter-rater agreement between the two observers. The agreements on lesion conspicuity, quality of fat suppression, and overall image quality were fair. The agreement on motion artifacts was moderate. The agreement on pulsation artifacts and homogeneity of blood vessel signal intensity were substantial, while the agreement on metal artifacts was almost perfect.

Discussion

CS-3D-T1TFFE imaging required shorter acquisition time than MS-SE (1 min 43 s and 5 min 56 s,

respectively) and showed no image degradation while maintaining equal or higher SNR and image quality. In the qualitative analysis, CS-3D-T1TFFE imaging was better than MS-SE in assessments of motion artifacts, pulsation artifacts, and homogeneity of blood vessel signal intensity. The short acquisition time for CS-3D-T1TFFE, which was only less than 30% of scan time for MS-SE, might have been effective in reducing motion artifacts. GRE sequences might have suppressed the artifacts created by pulsation or blood flow: in routine SE imaging, at least part of the reason for flow-related signal loss is that spins move out of the section between the two pulses. In GRE imaging, refocusing is performed by means of a gradient reversal, and short TE minimizes flow-related signal losses (13). In the head and neck region, since flow-related signal losses sometimes make it difficult to distinguish cervical lymph node from adjacent vessels, homogeneous blood vessel signal intensity might be helpful for detection of metastatic lymph nodes. The quality of fat suppression was significantly higher with MS-SE than with CS-3D-T1TFFE in assessments by Observer 2, whereas they were not significantly different between the methods in assessments by Observer 1. This difference between observers could be attributed to the fact that Observer 2 gave low scores for the deficient fat suppression by aliasing in the bottom near the supraclavicular slice in CS-3D-T1TFFE imaging (Fig. 6). Except for those slices, fat suppression in CS-3D-T1TFFE was entirely good: scores for all images were 4 (good) or 5 (excellent), with mean scores of 4.90 ± 0.31 and 4.67 ± 0.48 for Observers 1 and 2, respectively. The fat suppression was also

Table 2. Individual observer grades for MS-SE and CS-3D TITFE

	Observer 1			Observer 2		
	MS-SE	CS-3D-TITFE	<i>P</i> [*]	MS-SE	CS-3D-TITFE	<i>P</i> [*]
Degree of lesion conspicuity	4.90 ± 0.31	4.83 ± 0.46	0.4888	4.83 ± 0.38	4.80 ± 0.48	0.5725
Motion artifact	4.30 ± 0.88	4.90 ± 0.40	0.0009613	3.83 ± 1.02	4.53 ± 0.73	<0.0001
Metal artifact	4.20 ± 0.76	4.13 ± 0.78	0.1608	4.33 ± 0.71	4.33 ± 0.66	1
Pulsation artifact	3.43 ± 1.07	5	<0.0001	3.17 ± 1.23	4.97 ± 0.18	<0.0001
Quality of fat suppression	5	4.90 ± 0.31	0.08307	4.97 ± 0.18	4.67 ± 0.48	0.001426
Homogeneity of blood vessel signal intensity	1.80 ± 0.66	4.93 ± 0.25	<0.0001	1.60 ± 0.50	4.87 ± 0.35	<0.0001
Overall image quality	4.10 ± 0.76	4.20 ± 0.61	0.3256	4.10 ± 0.96	4.17 ± 0.70	0.6015

Values are given as mean ± SD.

*Paired *t*-test.

CS-3D TITFE, three-dimensional T1 turbo field echo with Compressed SENSE; MS-SE, multi slice spin echo; SD, standard deviation.

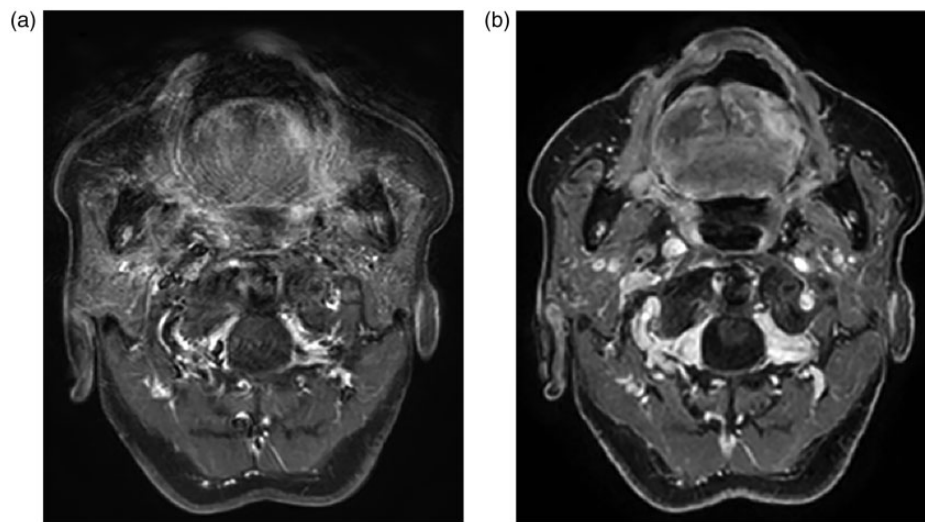


Fig. 3. Motion artifact: An 83-year-old woman with left tongue squamous cell carcinoma. Imaging was performed with the MS-SE sequence (a) and the CS-3D-TITFE sequence (b). The tongue lesion is difficult to be identified on the MS-SE image because of the heavy motion artifact, while the CS-3D-TITFE image delineates the lesion clearly. CS-3D-TITFE, three-dimensional T1 turbo field echo with compressed SENSE; MS-SE, multi-slice spin echo.

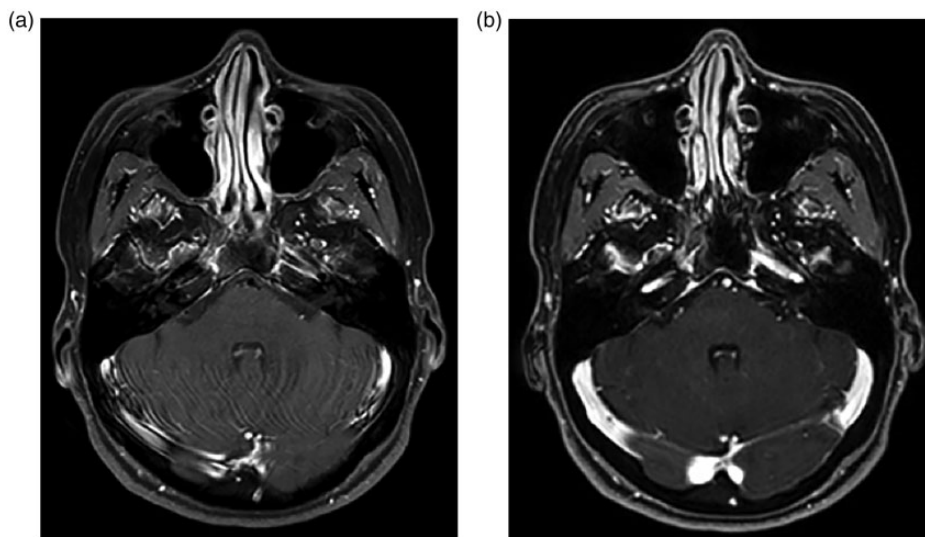


Fig. 4. Pulsation artifact: A 39-year-old woman with left maxillary desmoplastic ameloblastoma. Imaging was performed with the MS-SE sequence (a) and the CS-3D-TITFE sequence (b). The MS-SE image shows the flow-related artifact in the posterior cranial fossa. CS-3D-TITFE, three-dimensional T1 turbo field echo with compressed SENSE; MS-SE, multi-slice spin echo.

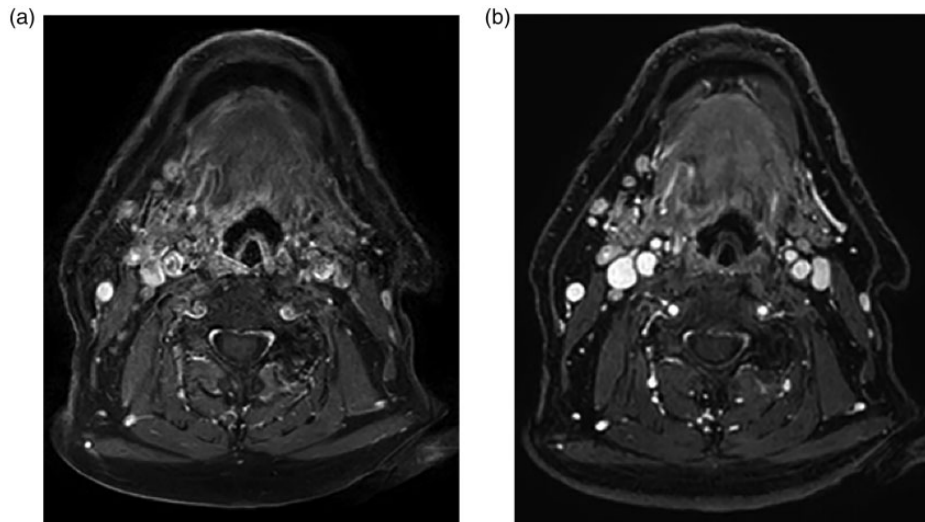


Fig. 5. Homogeneity of blood vessel signal intensity: An 81-year-old man with right tongue squamous cell carcinoma. Imaging was performed with the MS-SE sequence (a) and the CS-3D-TITFE sequence (b). The MS-SE image shows inhomogeneity of blood vessel signal intensity, while the CS-3D-TITFE image shows homogeneity. CS-3D-TITFE, three-dimensional T1 turbo field echo with compressed SENSE; MS-SE, multi-slice spin echo.

Table 3. Kappa statistics between two observers.

	Kappa statistics
Degree of lesion conspicuity	0.339
Motion artifact	0.416
Metal artifact	0.83
Pulsation artifact	0.759
Quality of fat suppression	0.38
Homogeneity of blood vessel signal intensity	0.796
Overall image quality	0.321

good around the skull base and the intraorbital regions that are susceptible to artifacts. We employed the two-point Dixon method for fat suppression (14). Dixon sequences can compensate the inhomogeneity of static magnetic field (B_0), thereby providing accurate separation between water and fat. The Dixon method provides us with water, fat, in phase, out of phase, and B_0 images; however, the water image that represents the fat-suppression image, is helpful for lesion conspicuity in contrast-enhanced MRI. Therefore, we used only the water images in this study.

There were no significant differences in metal artifacts, lesion conspicuity, and overall image quality. While the GRE sequence is more sensitive to field heterogeneity or metal-induced susceptibility artifacts than SE (15), there were no significant differences between the two sequences in the present study. This could have occurred because the aforementioned improved B_0 correction compensated the field heterogeneity and the use of a higher bandwidth in

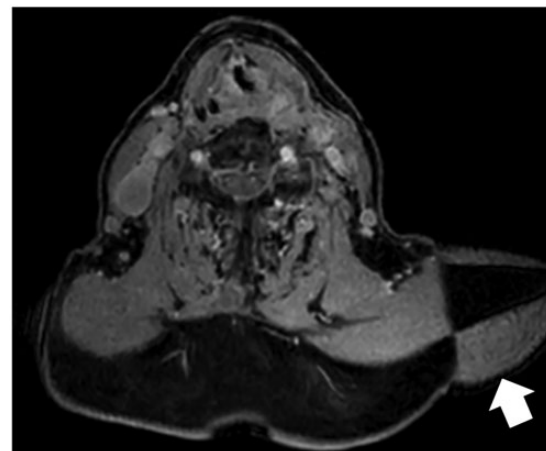


Fig. 6. A 77-year-old woman with right tongue squamous cell carcinoma. The image obtained by the CS-3D-TITFE sequence shows deficient fat suppression caused by aliasing in a near supraclavicular slice (arrow). CS-3D-TITFE, three-dimensional T1 turbo field echo with compressed SENSE.

CS-3D-TITFE reduced the distortion by the artifact (16,17). The increased bandwidth might cause decreased SNR, but the SNR of CS-3D-TITFE was kept equal or higher than MS-SE in our settings. Dental prostheses induce metal artifact, which often interferes with lesion conspicuity; the result showed that CS-3D-TITFE did not induce any worse effects in terms of forming metal artifact. The kappa statistics were fair or moderate in four out of seven parameters (degree of lesion conspicuity, motion artifact, quality of fat suppression, and overall image quality), even

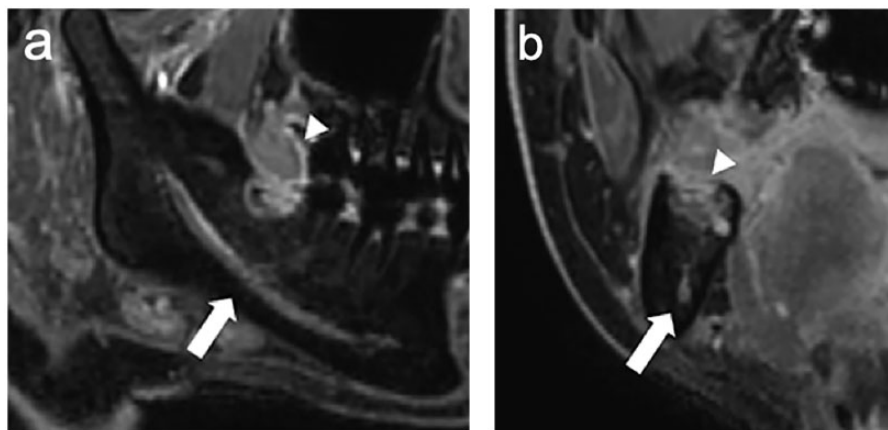


Fig. 7. A 35-year-old woman with inflammation after extraction of a right mandibular wisdom tooth. Reconstructed sagittal (a) and coronal (b) plane images from axial images of the CS-3D-T1TfE sequence shows the relationship between the inflamed region (arrow heads) and the mandibular canal (arrows) clearly. CS-3D-T1TfE, three-dimensional T1 turbo field echo with compressed SENSE.

though the actual scores (Table 2) appeared to be similar. Since, both the observers provided quite high grades for these four parameters, the skewed distribution of the data eventually resulted in fair or moderate kappa values.

We employed 3D scans with CS because there is more room for aggressive undersampling compared to 2D scans (12), and 3D imaging is particularly attractive as it is often time-consuming and reduction of scan time is a higher priority than 2D imaging. 3D imaging enables us to reconstruct the sagittal and coronal plane images from the original axial plane images. Fig. 7 shows the reconstructed sagittal and coronal plane images. We can see the positional relationship between the inflamed region and the mandibular canal clearly; however, more precise assessment of reconstructed images will be needed with more cases.

The present study has some limitations. First, the optimal CS-Sense reduction factor has not been examined. Moreover, the advantages of CS-Sense over the conventional SENSE were not examined. We chose the CS-Sense reduction factor to set an acquisition time that was lower than 2 min 47 s of the existing 2D non-enhanced T1-SE sequence without fat suppression that seemed to be a clinically important standard. Higher CS-Sense reduction factor could be used; however, it is associated with a greater risk of image degradation. To the best of our knowledge, CS-Sense reduction factor in the head and neck area that has many artifacts like oral prosthesis and air has not been studied previously. We had to be careful because the images were taken after the administration of contrast material. Thus, we chose the clinically acceptable setting rather than the fastest setting. Second, the numbers of cases in which each of the two sequences was

performed first after administration of contrast material were not the same, since MS-SE imaging was performed first in 20 cases while CS-3D-T1TfE imaging was performed first in 10 cases. This suggests that the condition was worse for CS-3D-T1TfE, but this study showed that CS-3D-T1TfE imaging was better or equal to MS-SE. Third, we did not evaluate the conspicuity of perineural growth and lymph nodes that may be subtle but can greatly impact the choice of therapy. This is an important aspect that requires further evaluation.

In conclusion, the CS-3D-T1TfE sequence was useful for oral and maxillofacial MRI: the acquisition time decreased to less than 30% of that for MS-SE without image degradation, maintaining equal or higher SNR and image quality, which led to throughput enhancement. There would be no need for additive sagittal and coronal plane image acquisition, which will lead to a further reduction in examination time.

Declaration of conflicting interests

The author(s) declared no potential conflicts of interest with respect to the research, authorship, and/or publication of this article.

Funding

The author(s) received the following financial support for the research, authorship, and/or publication of this article: This work was supported by JSPS KAKENHI (grant no. JP 19K10314).

ORCID iD

Yukiko Kami  <https://orcid.org/0000-0003-0092-7239>

References

1. Togao O, Hiwatashi A, Yamashita K, et al. Measurement of the perfusion fraction in brain tumors with intravoxel incoherent motion MR imaging: validation with histopathological vascular density in meningiomas. *Br J Radiol* 2018;91.
2. Chikui T, Kitamoto E, Kami Y, et al. Dynamic contrast-enhanced MRI of oral squamous cell carcinoma: a preliminary study of the correlations between quantitative parameters and the clinical stage. *Br J Radiol* 2015;88.
3. Dammann F, Bootz F, Cohnen M, et al. Diagnostic imaging modalities in head and neck disease. *Dtsch Arztebl Int* 2014;111:417–423.
4. Dhanuthai K, Rojanawatsirivej S, Thosaporn W, et al. Oral cancer: A multicenter study. *Med Oral Patol Oral Cir Bucal* 2018;23:23–29.
5. Jaspan ON, Fleysler R, Lipton ML. Compressed sensing MRI: a review of the clinical literature. *Br J Radiol* 2015;88.
6. Hamilton J, Franson D, Seiberlich N. Recent advances in parallel imaging for MRI. *Prog Nucl Magn Reson Spectrosc* 2017;101:71–95.
7. Deshmane A, Gulani V, Griswold MA, Seiberlich N. Parallel MR imaging. *J Magn Reson Imaging* 2012;36:55–72.
8. Geethanath S, Reddy R, Konar AS, et al. Compressed sensing MRI: a review. *Crit Rev Biomed Eng* 2013;41:183–204.
9. Lustig M, Donoho D, Pauly JM. Sparse MRI: The application of compressed sensing for rapid MR imaging. *Magn Reson Med* 2007;58:1182–1195.
10. Liang D, Liu B, Wang J, Ying L. Accelerating SENSE using compressed sensing. *Magn Reson Med* 2009;62:1574–1584.
11. Geerts-Ossevoort L, de Weerd E, Duijndam A, et al. Compressed SENSE. Speed done right. Every time. Philips Healthcare, Netherlands 2018. Available at: <https://philipsproductcontent.blob.core.windows.net/assets/20180109/619119731f2a42c4acd4a863008a46c7.pdf>.
12. Sartoretti E, Sartoretti T, Binkert C, et al. Reduction of procedure times in routine clinical practice with Compressed SENSE magnetic resonance imaging technique. *PLoS One* 2019;14.
13. Elster AD. Gradient-echo MR imaging: techniques and acronyms. *Radiology* 1993;186:1–8.
14. Dixon WT. Simple proton spectroscopic imaging. *Radiology* 1984;153:189–194.
15. Hargreaves BA, Worters PW, Pauly KB, et al. Metal-induced artifacts in MRI. *AJR Am J Roentgenol* 2011;197:547–555.
16. Ulbrich EJ, Sutter R, Aguiar RF, et al. STIR sequence with increased receiver bandwidth of the inversion pulse for reduction of metallic artifacts. *AJR Am J Roentgenol* 2012;199:735–742.
17. Lee MY, Song KH, Lee JW, et al. Metal artifacts with dental implants: Evaluation using a dedicated CT/MR oral phantom with registration of the CT and MR images. *Sci Rep* 2019;9:754.